Polymer 50 (2009) 881–890

Contents lists available at ScienceDirect

Polymer

journal homepage: www.elsevier.com/locate/polymer

Bio-nano complexes: DNA/surfactant/single-walled carbon nanotube interactions in electric field

HyungKi Lee, Jovan Mijović*

Othmer–Jacobs Department of Chemical and Biological Engineering, Polytechnic Institute of New York University, Six Metrotech Center, Brooklyn, NY 11201, USA

ARTICLE INFO

Article history:
Received 11 September 2008
Received in revised form
2 December 2008
Accepted 7 December 2008
Available online 16 December 2008

Keywords:
Deoxyribonucleic acid
Single-walled carbon nanotube
Dielectric relaxation spectroscopy

ABSTRACT

Bio-nano complexes of calf-thymus DNA with a cationic surfactant (DNA/DTAB) and with surfactant wrapped single-walled carbon nanotubes (DNA/SD) were prepared and investigated. The focus of this study was on the molecular interactions, dynamics and binding characteristics as evaluated by a battery of experimental techniques. The major binding sites on DNA and their binding affinities toward the surfactant (DTAB) are identified by Fourier Transform InfraRed (FTIR) spectroscopy. DTAB molecules display higher binding affinity toward DNA when hydrophobically attached to the single-walled carbon nanotube (SWNT) surface. Dielectric spectroscopy of the neat DNA and the two complexes revealed the presence of a process assigned to the motions of counterions distributed along the DNA backbone. The time scale of this process is a function of the composition of the complex and is shortest at a particular DNA/DTAB or DNA/SD ratio. The effect of SWNT on the zeta potential and the hydrodynamic diameter is manifested by the speed-up of charge reversal and a large complex size at the iso-electric point (IEP). The secondary structure of DNA is altered by the presence of SWNTs; however, there is no evidence of the transition of DNA in either complex from type B to other forms.

1. Introduction

Interaction of DNA with cationic surfactants and/or single-walled carbon nanotubes (SWNTs) has generated considerable excitement in recent years due to the growing interest in the application of such nanoscopic complexes in biological engineering and nano-biotechnology. Several inorganic nanomaterials, including nanotubes, nanocrystals and nanowires, have been identified as promising vehicles for various applications in biological and medicinal sciences [1–5].

Studies of DNA/surfactant complexes have focused on the interactions between polyelectrolytes and surfactants [6–8]. The binding of cationic surfactants to the oppositely charged DNA is a discharging process that induces condensation of the DNA into a compact structure [9]. The formation of DNA/surfactant complex is straightforward due to the well-defined binding sites on DNA and strong electrostatic interaction [10]. Gorelov et al. [11] and Dias et al. [12] argue that the cooperative binding of cationic surfactants to DNA is caused by the hydrophobic interactions between bound surfactant molecules that lead to phase separation at high DNA concentration. This cooperative nature of binding results in a lower critical aggregation concentration which is usually a few orders of magnitude below the critical micelle concentration (CMC) of the free surfactants [13].

Single-walled carbon nanotubes (SWNTs) have been considered as potential bio-carriers that can cross the cell membrane without imparting toxicity [14–16]. Carbon nanotubes can also serve as scaffolds on which DNA molecules can be oriented, manipulated, and investigated without the need for chemical treatment. DNA immobilization platforms use high-resolution detection tips of carbon nanotubes for probing DNA fragments [17,18]. The formation of DNA/SWNT complexes is of interest for application in the biosensor field [19] for DNA hybridization detection [20], targeting [21], biocompatibility [22], etc. Zheng et al. [23] reported a direct association of DNA with SWNT, and showed that SWNTs in aqueous solution can be effectively dispersed by wrapping single-stranded DNA on SWNT based on the interaction strength developed by π-stacking. Remarkable electrical properties of SWNTs are of interest for the development of molecular-based electronic devices owing to the selective binding of complementary DNA strands onto nanotube surfaces [24]. Feazell et al. have demonstrated that carbon nanotubes can deliver cancer-targeting drugs, proteins and DNA into cells [25,26]. PrimeGen, a biotech company from California used SWNTs to introduce proteins into human testicular and retinal cells at an astonishing acceptance rate of 80% [27]. Xin et al. [28] reported DNA-templated assembly of surfactant wrapped

* Corresponding author. Tel.: +1 718 260 3097; fax: +1 718 260 3125.
E-mail address: jmijovic@poly.edu (J. Mijović).

0032-3861/$ – see front matter © 2008 Elsevier Ltd. All rights reserved.
doi:10.1016/j.polymer.2008.12.021

SWNT on the treated silicon substrate and suggested the use of DNA–SWNT assembly as a nanowire in nanoelectronic circuits.

The research described in this article is aimed at establishing the nature of interactions of DNA with DTAB or DTAB wrapped SWNTs during the complex formation. These interactions remain incompletely understood and no comprehensive study on this subject has been reported. More specifically, our principal objective is to understand the binding mechanism and dynamics of these bio-nano complexes under applied electric field. This is accomplished by the application of various experimental techniques that include dielectric relaxation spectroscopy (DRS), Fourier Transform InfraRed (FTIR) spectroscopy, zeta potential and circular dichroism (CD).

2. Experimental

2.1. Materials

Calf-thymus DNA (double stranded, ~20 kb, GC 41.9%, D4522) and dodecyltrimethylammonium bromide (DTAB) were obtained from Sigma–Aldrich. The AP grade (70% purity) single-walled carbon nanotubes (SWNTs) were obtained from Carborex and used without further purification. The effect of impurities on interactions with DNA cannot be excluded although even highly purified SWNTs contain up to 10% impurities. The DNA samples were prepared in pure deionized water and the concentration was determined using UV spectroscopy at the wavelength of 260 nm. DTAB wrapped SWNT solutions (SD) were prepared by homogenization with sonication followed by centrifugation. 10 mg of SWNTs were added to 50 mL of ionized water including 1% DTAB. This solution was sonicated for 24 h. A sonicator (model: UP-50H with sonotrode MS2, Hielscher Ultrasonics) with operating frequency of 30 kHz and maximum power output of 50 W was used for sample preparation. This suspension was centrifuged for 30 min at 13,000 rpm to remove the unbound SWNTs and the supernatant was then decanted. The decanted suspension remains stable for over 3 months.

2.2. Preparation of complexes

DNA/DTAB and DNA/SD complexes were prepared in 1.5 mL snap-cap tubes by adding DNA solution into SD or DTAB solution at various concentrations. For DRS and FTIR measurements, all samples were homogenized by sonicator in an ice-water bath for 1 min. The amount of DTAB in the solution was kept below the critical micelle concentration (CMC). The effect of DTAB above the CMC on the property of the complex was not considered in this study. Table 1 summarizes the samples investigated and specifies their codes.

2.3. Techniques

IR spectra were obtained on a Magna IR 750 spectrophotometer with a total of 100 scans and a resolution of 4 cm^{-1}. The collected spectra were manipulated using OMNIC software. A drop of sample solution on AgCl window was dried for 3 h in the refrigerator. The relative absorbance intensity of all major IR bands was determined by normalizing with respect to the internal reference peak at 966 cm^{-1}, due to deoxyribose C–C and C–O stretching vibrations, that show no spectral changes as a function of the weight ratio of the components. Dielectric measurements were performed on a Novocontrol α-high-resolution dielectric analyzer (3–7 MHz) equipped with heating/cooling controls, including Novocontrol's Novocool system custom-modified for measurements at low and high frequency. A detailed description of our facility has been given elsewhere [29–31]. Measurements of the Zeta potential and complex size were performed using a Zeta sizer Model ZS-90 (Malvern Instrument, Southborough, MA) at room temperature. At least five mean values were obtained for each sample. All samples were sonicated for homogenization and incubated in the refrigerator for 1 h before the measurements for the equilibrium complex formation. CD spectra were obtained using Jasco J-815 spectropolarimeter (Easton, MD) with a 10 mm path length rectangular cuvette cell at 25 °C. Spectra were recorded in the wavelength range from 350 to 210 nm at a scan rate of 1 nm/min and a resolution of 0.1 nm. Four spectra were collected and averaged for each sample. The minimum DNA concentration in all samples was 40 μg/mL.

Table 1
Sample description and codes.

Description	Codes
Deoxyribonucleic acid	DNA
Single-walled carbon nanotube	SWNT
Dodecyltrimethylammonium bromide	DTAB
Dodecyltrimethylammonium bromide wrapped single-walled carbon nanotube	SD
Complex formed by the interaction of DNA with DTAB	DNA/DTAB
Complex formed by the interaction of DNA with SD	DNA/SD

3. Results and discussion

Our working strategy consisted in applying a battery of experimental techniques to explore the character of DNA complexes and to establish the role of DTAB wrapped SWNTs in the complex formation. The paper is organized as follows. We begin by characterizing the neat DNA and the two DNA complexes DNA/DTAB and DNA/SD. We then proceed to examine the binding characteristics, relaxation and counterion dynamics, the zeta potential and the secondary structures of all systems investigated.

3.1. Characterization

3.1.1. Neat DNA and DTAB wrapped SWNTs

The original DNA sample was a double stranded helix of high molecular weight (~13,000 kDa or 20 kb) and heterogeneous size distribution. DNA samples were sonicated before each measurement to reduce the length and homogenize the solution. The final average size of the DNA was estimated at around 500 base pairs (bp) using gel-electrophoresis as shown in Fig. 1. The chemical structure of DTAB and a schematic of DTAB wrapped SWNTs (SD) are presented in Fig. 2. DTAB consists of a single hydrocarbon tail (Fig. 2a) with short chain length [32] which is hydrophobically attached to the SWNTs as shown in Fig. 2b. The stability of SD solutions was maintained for over 3 months at room temperature. The hydrodynamic diameter and the zeta potential of SD were determined to be 150 nm and +53 mV, respectively.

3.1.2. DNA complexes

We begin by examining the IR spectra of the neat DNA and various complexes. Double stranded (ds) calf-thymus DNA has major absorption bands in the mid-IR region between 650 and 1800 cm^{-1}. Specifically, the characteristic spectral bands in the neat DNA (bottom trace in Fig. 3a and b) appear at 1662 (thymine), 1608 (adenine), 1498 (cytosine), 1225 cm^{-1} (the asymmetric stretch of backbone phosphate) and, 1086 and 835 cm^{-1} (symmetric PO_2 stretch resulting from in-plane vibrations) [33]. The structural marker band for the calf-thymus ds-DNA is the absorbance peak at 1709 cm^{-1}, which is attributed to the C=O stretching mode of the base-paired residues. The disappearance of this band provides the

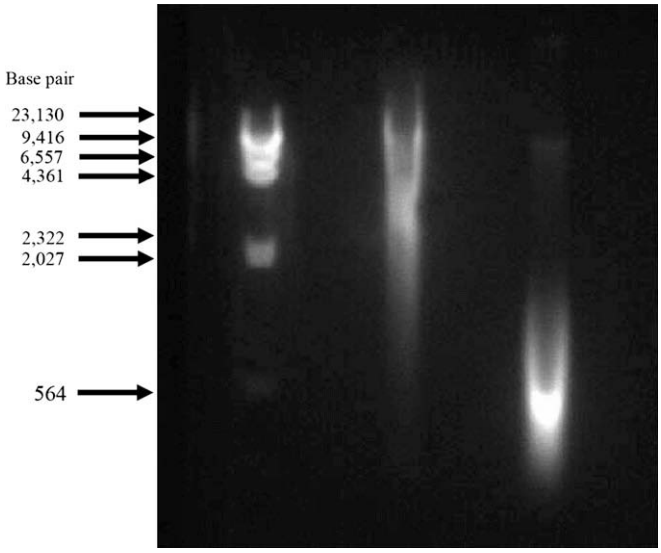

Fig. 1. DNA molecular weight standard (left), electrophoresis of the original DNA (middle) and DNA after 1 min sonication (right).

spectral criterion for the denaturation of ds-DNA [34]. Since the DNA helix has distinctive IR bands that afford identification of the secondary conformation changes, the effect of DTAB and DTAB wrapped SWNTs on the DNA structure can be gleaned from the IR spectra by examining the intensity of those peaks and their shift in the frequency (wavenumber) domain. Fig. 3a and b contains the IR spectra of DNA/SD and DNA/DTAB complexes, respectively, with the weight ratio as a variable, plotted on the right ordinate. We observe a shift of major spectral bands to higher wavenumber in both DNA/SD and DNA/DTAB complexes even at the lowest SD and DTAB loading (1.25 and 1.67 respectively). Moreover, the intensity of those bands decreases with increasing weight ratio. The structural marker band of DNA at 1709 cm^{-1} remains visible in the absorbance spectra with only a slight shift with increasing weight ratio and there is no evidence of a new band at 1692 cm^{-1} which has been attributed to the carbonyl vibrations of the unstacked bases [35]. A decrease in the intensity of bands at 1709 and 1662 cm^{-1} is due to a partial stabilization of the helix that results from the DTAB-phosphate binding. The presence of a peak at 1709 cm^{-1} in all spectra is a proof that the DNA is not denatured by DTAB at the weight ratios used in this study and that it remains in the double stranded helical configuration by maintaining the base stacking and pairing. The addition of DTAB results in the appearance of two new absorbance bands at 1482 and 1471 cm^{-1}, due to CH_2 symmetric bending, and the intensity of those peaks increases with increasing weight ratio as shown in Fig. 3. The addition of SWNT does not give rise to new bands in the DNA/SD spectra though it has an effect on the absorbance intensity and the wavenumber shift.

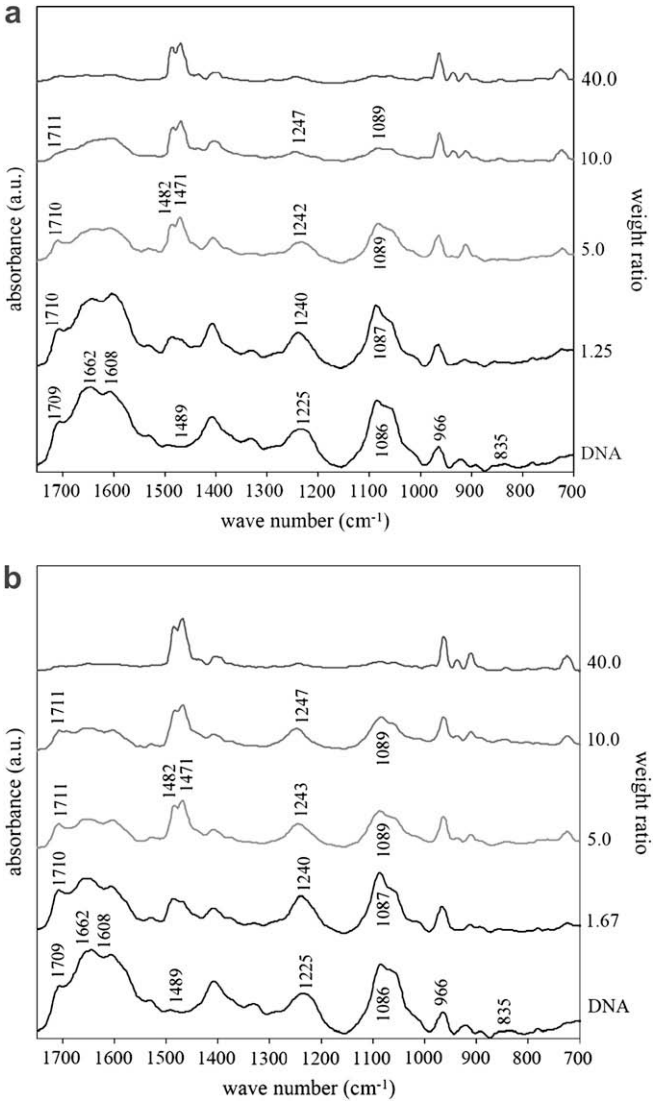

Fig. 3. IR spectra of (a) DNA/SD complex and (b) DNA/DTAB complex with weight ratio (SD:DNA or DTAB:DNA) as a variable.

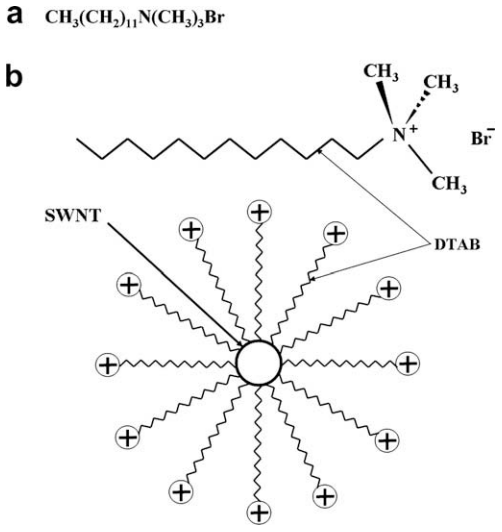

Fig. 2. (a) Molecular formula of dodecyltrimethylammonium bromide (DTAB) and (b) schematic representation of DTAB and DTAB wrapped single-walled nanotube (SWNT) (head on view).

Next, the relative intensity of the major absorbance bands at 1709, 1225 and 1086 cm^{-1} with the weight ratio as a variable was calculated using the peak at 966 cm^{-1} as internal reference. These three bands represent the base pairing (1709 cm^{-1}) and the stretch vibrations of the DNA phosphate backbone (1225 and 1086 cm^{-1}) where the main binding interactions between DNA and DTAB (or SD) take place. As shown in Fig. 4, the relative intensity systematically decreases with increasing weight ratio, indicating that the variation in the absorbance spectra is directly affected by the surfactant concentration.

The extent of binding to the surfactant also depends on the DNA/SD weight ratio. Two sets of DNA/SD complexes were examined in

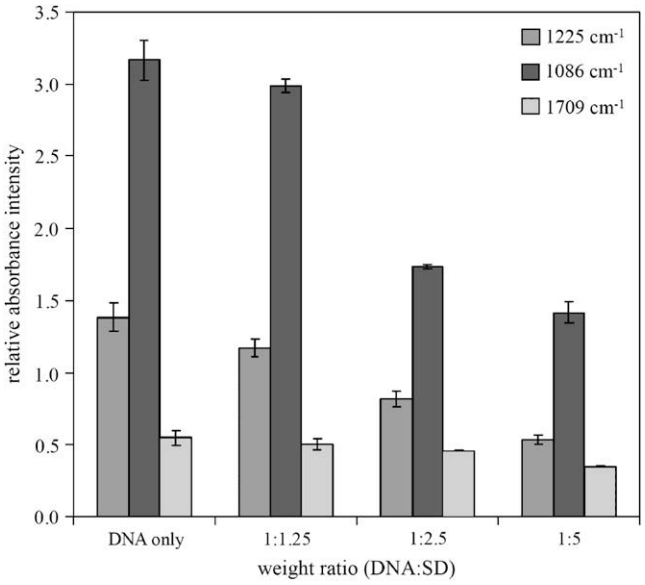

Fig. 4. Relative absorbance intensity of major bands in DNA/SD complex as a function of weight ratio (DNA:SD).

order to evaluate the extent of saturation of SD with DNA as captured by the IR spectra. With DNA in excess (SD:DNA = 1:2.5), the complex and the supernatant exhibit all major absorbance bands (at 1709, 1225 and 1086 cm^{-1}, etc.), indicating that the binding is unsaturated (Fig. 5a). On the other hand, at high SD concentration (SD:DNA = 1:1), the complex maintains the characteristic DNA bands, as shown in Fig. 5b, but the supernatant deviates from the original DNA fingerprint. This is because the DNA molecules in the complex are associated with SD and settle down during centrifugation. Simultaneously, we record the emergence of the characteristic DTAB absorption bands at 1482, 1471 and 911 cm^{-1}.

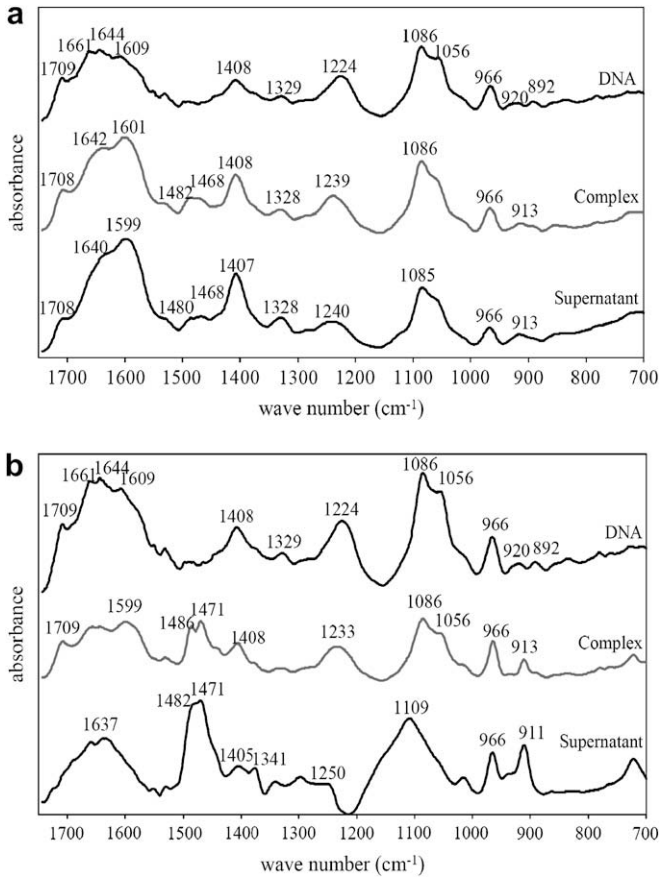

Fig. 5. Comparison of IR spectra of neat DNA with its complex and supernatant for the weight ratio (a) SD:DNA = 1:2.5 and (b) SD:DNA = 1:1.

3.2. Binding behavior

The binding affinities of SD and DTAB toward DNA are examined next. The calculation of the binding constants of DNA/SD and DNA/DTAB complexes was also carried out using the FTIR spectra. The relative intensities of the major bands at 1709 and 1086 cm^{-1} were calculated for each SD and/or DTAB concentration using the band at 966 cm^{-1} as a reference [36]. In order to obtain the relative intensity, the area for the specific bands (ex: 1709, 1086, reference, etc.) is calculated first. In the case of overlapping (shoulder and neighboring) bands extrapolation and deconvolution were utilized. This procedure is effectively conducted with the operating software (OMNIC). The relative intensity was then obtained by dividing the area of the target band with that of the reference band. The calculated binding constants for those two specific binding sites were plotted as a function of SD or DTAB concentration in Fig. 6. The calculation procedure has been described in the literature [37–39]. The binding constants of DNA/SD and DNA/DTAB complexes are defined as follows:

$$\mathrm{SD} + \mathrm{DNA} \leftrightarrow \mathrm{SD:DNA} \quad \mathrm{DTAB} + \mathrm{DNA} \leftrightarrow \mathrm{DTAB:DNA} \tag{1}$$

$$K_1 = [\mathrm{SD:DNA}]/[\mathrm{SD}][\mathrm{DNA}] \quad K_2 = [\mathrm{DTAB:DNA}]/[\mathrm{DTAB}][\mathrm{DNA}]$$

Fig. 6a and b shows how the major binding sites at 1709 and 1086 cm^{-1} are affected by SD (Fig. 6a) and DTAB (Fig. 6b). Note that the binding constant for the DNA/SD complex, K_1 (for both binding sites at 1709 and 1086 cm^{-1}) is higher than that for the DNA/DTAB complex, K_2 (for the corresponding binding sites), indicating a higher affinity of SD toward DNA. This is an interesting observation that is rationalized as follows. In the DNA/DTAB complex, free DTAB molecules bind to DNA through electrostatic attraction. Hydrophobic–hydrophobic interactions between the DTAB molecules bound to DNA and those present in the surrounding medium promote the formation of DTAB bi-layers that become a part of the DNA/DTAB complex. In the DNA/SD complex, on the other hand, there are micelle-like SDs that consist of DTAB molecules hydrophobically anchored on SWNTs (see Fig. 2b). The distribution of surfactants on a hydrophobic SWNT surface can be considered a monolayer as well as micelle-like form. Here, the electrostatic interaction between DNA and SD is the major driving force for the complex formation, although dissociated uncharged SWNTs, particularly at a low weight ratio, may adsorb onto DNA ends through hydrophobic interactions. DTAB molecules emanate radially from the SWNT surface and are favored to associate with the DNA molecules, thus accelerating the complex formation. The higher binding affinity of SD toward DNA is attributed to the fact that SD, due to its micellar structure, provides DNA with larger specific interactions than DTAB. Moreover, any reversible characteristic of surfactant adsorption was not observed within the measurable time scale.

The question of whether the ds-DNA will bind to the surface of uncharged SWNTs in solution has not been resolved by experimental or computational studies. In most experimental studies, SWNTs were modified with carboxylic end groups to facilitate solubilization in aqueous media and enhance electrostatic interactions with DNA. Li et al. [40] reported strong interactions

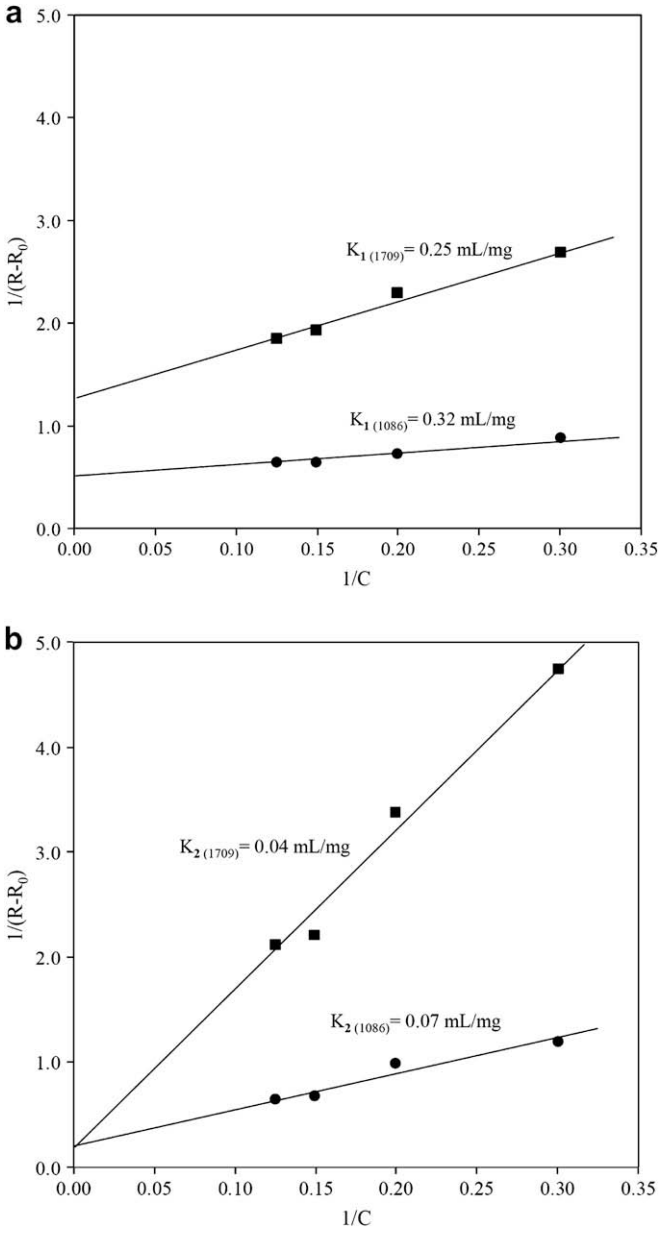

Fig. 6. Plot of $1/(R - R_0)$ vs. $1/C$ for (a) DNA/SD complex and (b) DNA/DTAB complex. R_0 is the initial relative intensity of major IR band and R is the recorded relative intensity as a function of DTAB concentration (C). The binding constants (K_1 and K_2) were determined for the bands at 1709 and 1086 cm^{-1}.

between the open end functionalized SWNT and the major groove of DNA and demonstrated a fluorescence binding assay where SWNTs bind to DNA by excluding the binders out of their binding sites. Zhao et al. [41] conducted a computational study and showed that SWNTs are able to attach to the hydrophobic end groups of DNA but not to the hydrophilic DNA backbone. In our study, SWNTs do not have carboxylic end groups but are wrapped instead by cationic surfactants which enhance their solubilization in aqueous media. Hydrophobic interactions occur between the uncharged SWNT surface and DNA at lower weight ratio (SD:DNA). The difference in the binding affinity between SD and DTAB as expressed in terms of K ($K_{DNA/SD} > K_{DNA/DTAB}$) is due to this hydrophobic association of SWNT with DTAB as well as the interaction between free uncharged SWNT and DNA. Since DNA/SD and DNA/DTAB solutions contain the same amount of DTAB, one may expect the same electrostatic potential of DTAB. But, we observe a distinctly higher affinity of DNA/SD complex in comparison to DNA/DTAB and take that as a proof that SWNTs play a significant role in the binding interaction between DTAB and DNA.

3.3. Relaxation and migration dynamics in DNA complexes

Thus far we have shown that the IR absorbance bands arising from the specific sites on DNA are affected by the binding with surfactant and the presence of SWNT. The electrostatic interaction between the DTAB and the DNA phosphate group is the main driving force for the complex formation and is stronger in DNA/SD than DNA/DTAB complex. It is of further interest to examine the electrostatic properties of the DNA complexes using dielectric relaxation spectroscopy (DRS) in order to evaluate the response of charged components to the applied electric field. For polyelectrolytes in aqueous solution, the fluctuation of counterions along the polyelectrolyte is believed to provide the key contribution to the dielectric response at frequencies below 1 MHz [42,43]. The dielectric response in this frequency region is not caused by the rotation of the permanent dipole moment of the entire DNA molecule but originates instead from the polarization of condensed counterions along an essentially stationary polyelectrolyte chain [44,45].

DRS spectra were generated over a wide range of temperature and frequency. The complex dielectric permittivity is defined as $\varepsilon^* = \varepsilon'(\omega) - i\varepsilon''(\omega)$ where $\varepsilon'(\omega)$ is the real permittivity, $\varepsilon''(\omega)$ is the dielectric loss factor and $\omega = 2\pi f$ (Hz). Dielectric spectra in the frequency domain contain information about many orders of magnitude of time scales and length scales of motion of various charged species in the electric field. In the text below we refer to the characteristic time constant obtained from the dielectric loss spectra as 'relaxation time', while acknowledging that this parameter should not be confused with the time scale of the segmental motions (the alpha process) in glass formers. As we shall see, the average 'relaxation time' in this study corresponds to the time scale of motions that result from the fluctuations of counterions surrounding the DNA backbone. We examine the dielectric response of the neat DNA first. Calf-thymus DNA exhibits two dielectric loss peaks in the frequency domain between 0.1 Hz and 1 MHz as shown in Fig. 7a. The low frequency peak (LFP) is due to the frozen water molecules in the DNA–water matrix, and the high frequency peak (HFP) is attributed to the counterion fluctuation along the DNA chains [46–48]. For the LFP, an Arrhenius plot of the average relaxation time vs. reciprocal temperature yields the value of activation energy of 55 kJ/mol, the same as pure ice [49]. The HFP has lower activation energy of 24 kJ/mol (Fig. 7b). Both peaks shift to lower frequency with decreasing temperature as shown in Fig. 7a. In this work, we focus on the HFP which represents the dielectric response arising from the counterions distributed along the DNA phosphate backbone [50,51].

We consider in more detail the dielectric response of DNA/SD complexes at frequencies below 10^6 Hz and temperature between −80 and 10 °C. We reiterate that no significant difference in the dielectric response of DNA/SD and DNA/DTAB is observed. The average relaxation time for the DNA/SD complex, obtained from the fits of the loss spectra to the well-known Havriliak–Negami (HN) functional form [52–56], is plotted as a function of the SD:DNA weight ratio with temperature as a parameter in Fig. 8. At any given temperature, the time scale of this process decreases with increasing SD concentration until the weight ratio of about 10 and then it starts to increase. Apparently, there exists a specific weight ratio where this process is fastest and an explanation of that observation is as follows. Negatively charged DNA molecules in the solution are surrounded by positive counterions leading to: 1) the

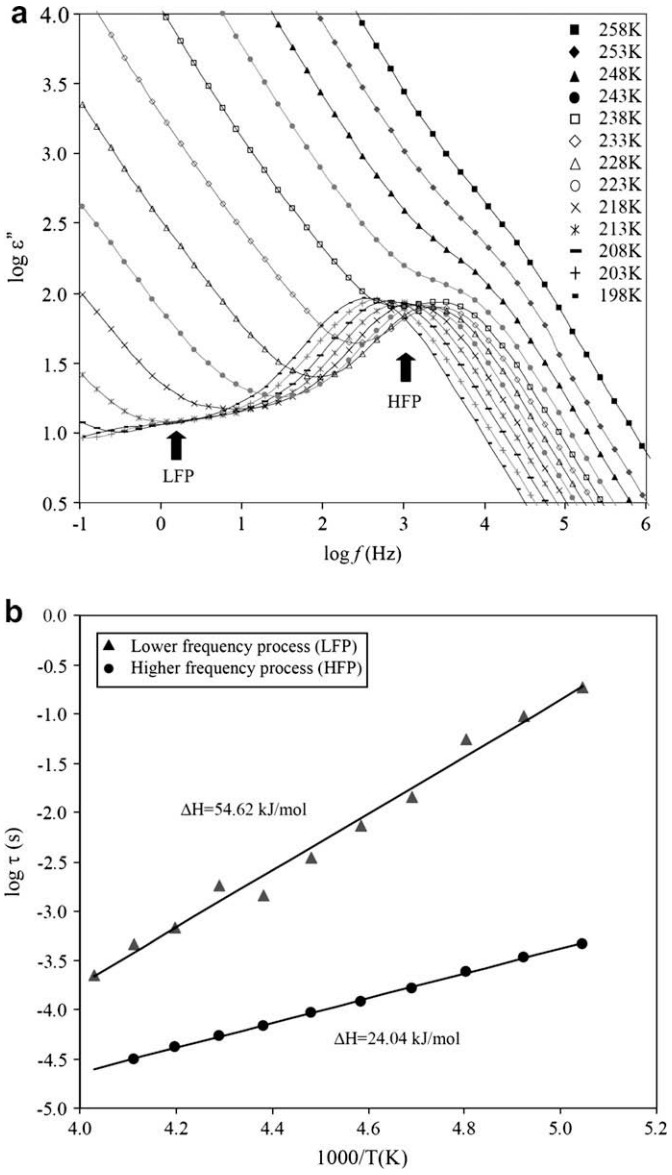

Fig. 7. (a) Dielectric loss in the frequency domain (note peaks at lower (LFP) and higher (HFP) frequency) and (b) temperature dependence of the average relaxation time for DNA solution (1 mg/mL).

formation of electrostatically driven clouds in the proximity of the DNA chains and 2) the compaction of DNA molecules [57]. In the presence of DTAB, strong electrostatic attractions between the DNA and the surfactant result in the formation of a complex whereby the counterions along the DNA backbone are replaced with surfactant. The other charged species that include the free surfactant, counterions and coions, are distributed around this complex in accordance with the Boltzmann distribution [58]. The dielectric response described in Fig. 8 reflects the behavior of counterions that surround the complex and exhibit fastest dynamics at a specific weight ratio. We shall revert to the discussion of this phenomenon later in the text.

The shape of the counterion cloud surrounding a DNA/SD or a DNA/DTAB complex varies depending upon the charge density on the complex [59,60]. The non-uniformly distributed charges on the complex induce a dipole moment in the applied electric field [61]. This induced dipole moment in a DNA solution is expressed as $\vec{\mu} = \alpha V \vec{E}$, where α is the polarizability of the molecule per unit

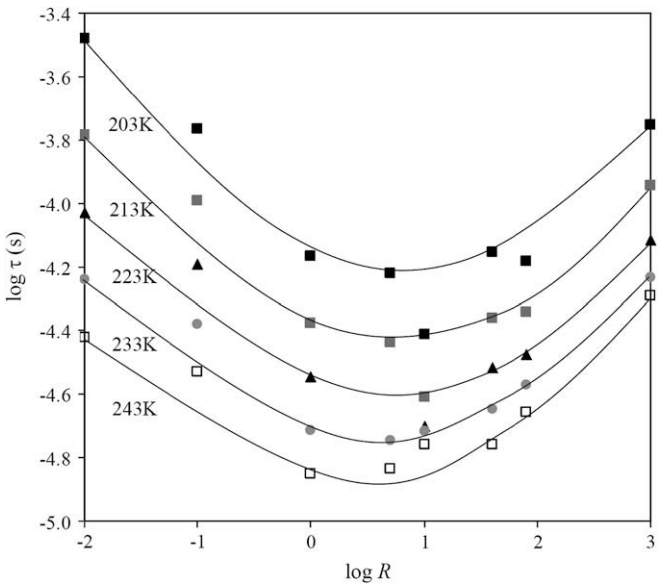

Fig. 8. Average relaxation time of DNA/SD complex as a function of weight ratio R with temperature as a variable.

volume; V is the volume; $\vec{E}$ is the electric field [62]. The dielectric relaxation time depends on the friction coefficient for the condensed counterions that move along the DNA backbone according to the following expression [63]:

$$\tau \approx \frac{\xi L^2}{6kT} \approx \frac{\xi}{6kT} N^2 b^{10/7} f^{8/7} l_B^{4/7} \quad (2)$$

where ξ is the friction coefficient for condensed counterions moving along the stationary polyion backbone; L is the chain contour length; k is the Boltzmann constant, T is temperature; N is the number of condensed counterions; b is the monomer size (0.43 nm); f is the fraction of monomer bearing an effective charge; l_B is the Bjerrum length (0.71 nm).

As seen from Eq. (2), the relaxation time is directly proportional to N, f and ξ. The counterion distribution on the complex is important in determining the relaxation time and is governed by the fraction of effectively charged monomer and the number of condensed counterions. The non-linear dependence of the average relaxation time on the weight ratio is due to two factors: 1) higher molecular weight of DNA in comparison to DTAB, and 2) non-uniform counterion distribution on the complex. The first factor is intuitively obvious. The average molecular weight of ds-DNA is approximately 3×10^5 Da (500 bp), about 1000 times that of DTAB, resulting in a large available binding interface. The effect of the non-uniformity of the counterion distribution is reflected as follows. At the lowest weight ratio, the charge distribution of the complex is dominated by the DNA counterions and the effect of DTAB on the overall charge is negligible, suggesting a nearly homogeneous charge distribution with low degree of polarizability. As the weight ratio increases, an increasing number of DNA counterions is replaced by DTAB through electrostatic binding interactions, and that creates a gradually increasing non-uniform charge distribution. The degree of non-uniformity reaches a maximum at the weight ratio between 1 and 100 which is well below the condition where DNA counterions are fully replaced by DTAB and charges are neutralized. The non-uniform charge distribution of negative and positive counterion clouds induces higher polarizability. The large induced dipole moment at the weight ratio of around 10 is responsible for fast relaxation due to the larger electrostatic torque exerted on the complex. Khachatourian et al.

reported that the electrostatic torque is a direct consequence of the Coulomb forces acting on an asymmetric distribution of charges residing on the surfaces of spheres [64]. As seen in Fig. 8, as the weight ratio increases over 100, the average relaxation time begins to increase since polarizability decreases as the consequence of a lower degree of non-uniformity in charge distribution at higher number density of DTAB or SD. Our results clearly demonstrate that the relaxation time is sensitive to the weight ratio (DTAB:DNA or SD:DNA).

Fig. 9 shows how the activation energy of the DNA/SD complex varies with the weight ratio. Based on the electrostatic binding model of Manning (1978) and Rouzina and Bloomfield (1997) [65], the free energy of cations binding to DNA is expressed as follows:

$$\Delta G = -zRT \ln(N_s/N) \quad (3)$$

where z is the valence number of cations, R is the gas constant, T is temperature in kelvin, N_s is the maximum counterion concentration at the DNA surface and N is the molar concentration of added monovalent cations.

In our samples, only two ionic components are added to the solution: the surfactant and the DNA. We define the molar concentration of DTAB as N and use it to estimate the free energy of cationic binding to DNA. In Eq. (3), N_s is calculated to be 1 M for a long DNA [66]. As the surfactant concentration increases, the free energy of binding (ΔG) decreases. ΔG is directly proportional to the surface charge density of DNA. While the binding sites on DNA are being occupied by the cationic head groups (DTA^+) through electrostatic interaction, the overall charge density of DNA decreases resulting in the decrease of binding energy. When DNA concentration exceeds DTAB concentration, ΔG becomes negative indicating that the binding of DTAB to DNA is favored. This binding energy effectively lowers the activation energy and stabilizes the complex as DTAB binds to DNA even more tightly. The lower binding energy at the highest weight ratio (SD:DNA or DTAB:DNA) indicates that strong binding interaction requires lower activation energy.

3.4. Zeta potential and hydrodynamic diameter

In an applied electric field, charged species are attracted to the electrode of the opposite polarity resulting in an electrostatic potential, called the zeta potential. The zeta potential of a complex is determined by the charge ratio between the DNA and the surfactant. Calf-thymus DNA in pure deionized water has a highly negative zeta potential (−77 mV) owing to the phosphate groups on its backbone. For polyelectrolyte molecules in aqueous media, the zeta potential is affected by the presence of a non-uniform charge distribution and the amount and type of counterions present in the solution.

The zeta potential and the hydrodynamic diameter of DNA/DTAB and DNA/SD complexes in pure deionized water were measured as a function of weight ratio (DTAB:DNA or SD:DNA) at 25 °C using electrophoresis and dynamic light scattering. The diameter measured by dynamic light scattering is determined from the translational diffusion coefficient using the Stokes–Einstein equation. The hydrodynamic diameter of a non-spherical complex corresponds to the diameter of a sphere that would have the same translational diffusion coefficient.

DNA/DTAB complex is examined first. As shown in Fig. 10a, the zeta potential of the DNA/DTAB complex (right ordinate) is −42 mV at the weight ratio of 10. The zeta potential decreases toward zero with increasing weight ratio and reaches plateau at the weight ratio

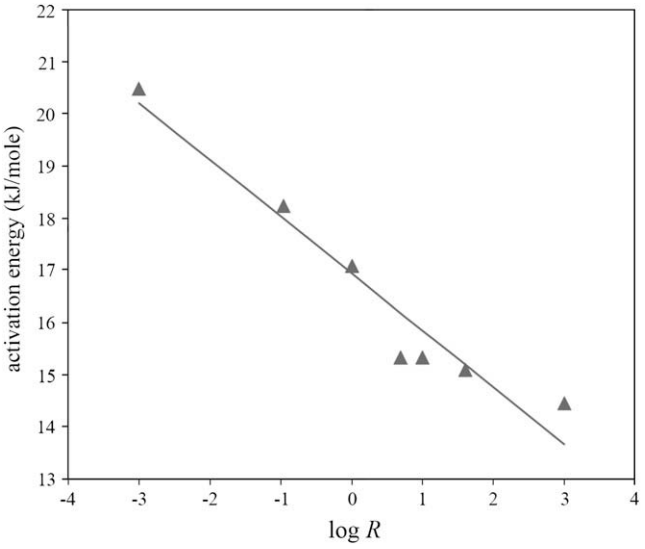

Fig. 9. Activation energy of DNA/SD complex as a function of weight ratio R (SD:DNA). Activation energy was obtained from fits of dielectric relaxation time vs. reciprocal temperature.

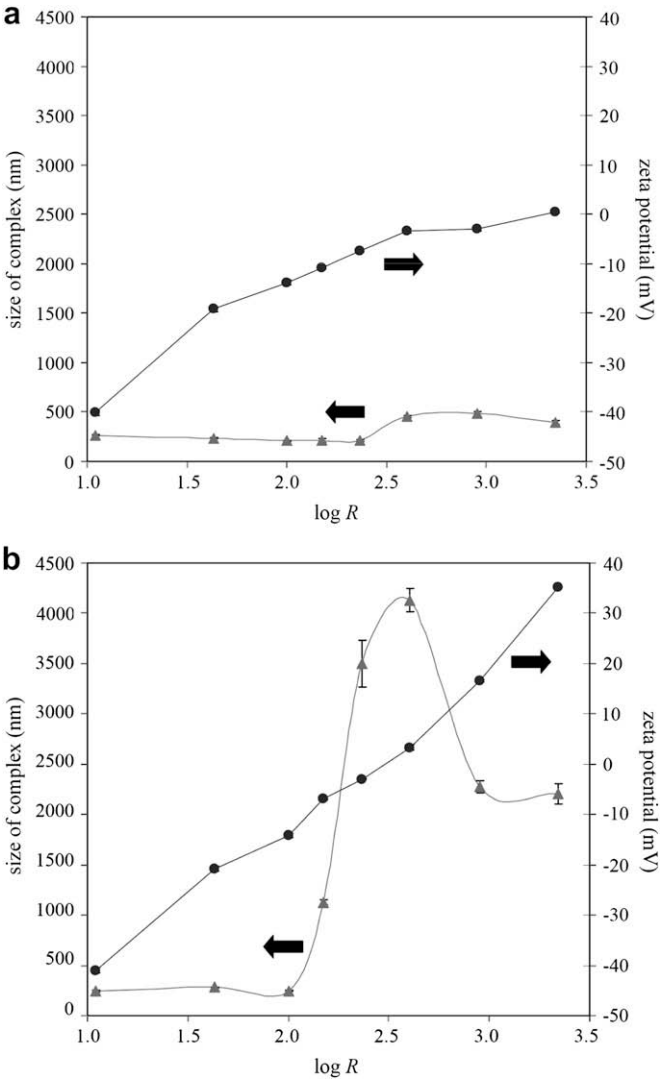

Fig. 10. Zeta potential (right ordinate) and complex size (left ordinate) of (a) DNA/DTAB and (b) DNA/SD complexes as a function of weight ratio R (DTAB:DNA or SD:DNA).

of about 400. This plateau corresponds to the iso-electric point (I.E.P) where the negatively charged DNA is neutralized by the cationic surfactant. The free DTAB molecules adsorb onto the DNA backbone electrostatically with their hydrophobic tails pointing outward. This further leads to the hydrophobic attraction between DTAB molecules, resulting in the formation of DTAB bi-layers between DNA molecules. But once the DTAB molecules replace all counterions on the DNA phosphate backbone, we observe no charge reversal process in the zeta potential measurement. This is attributed to the fact that the free DTAB molecules are not recognized as particles and hence do not contribute to the positive zeta potential because they do not have any electrophoretic mobility under applied voltage.

With respect to the size of the complex (left ordinate, Fig. 10a), note that the hydrodynamic diameter of the DNA/DTAB complex is about 250 nm at the lowest weight ratio and it decreases slightly until the weight ratio reaches 300 nm. The decrease in the hydrodynamic diameter with increasing weight ratio implies that the DNA/DTAB complex assumes a more condensed form due to the binding interactions while the counterions on the DNA backbone are replaced by DTA^+ cations. Mel'nikov et al. [67,68] used fluorescence microscopy and observed DNA compaction upon the addition of a cationic surfactant. They showed how DNA molecules change from the extended coil to the compacted globular state in the presence of a surfactant. In our study, the size of the complex increases with increasing weight ratio and reaches a broad peak at about 600 nm. This value corresponds to the I.E.P where the attraction forces between DTAB and DNA are strongest due to the weak electrostatic repulsion. The implication is that the overall complex formation is dominated by the electrostatic interaction between DTAB and DNA.

We next turn attention to the results for the DNA/SD complex described in Fig. 10b. The zeta potential of the DNA/SD complex at the weight ratio of 10 is identical to that of the DNA/DTAB complex. Furthermore, the decrease in the zeta potential up to −15 mV mimics that in the DNA/DTAB complex. At a low weight ratio, SD splits into DTAB and SWNT because the concentration of DTAB in the solution is diluted by the addition of DNA in deionized water. The free DTAB molecules adsorb onto DNA backbone electrostatically while the separated SWNTs attach hydrophobically to the DNA end groups. Consequently, the variation of the zeta potential for the DNA/DTAB complex parallels that of the DNA/SD complex at a low weight ratio. But that is where the similarities end because the zeta potential in the DNA/SD complex does not level off past the I.E.P. Instead, it continues to increase with SD concentration while the charge of the DNA/SD complex undergoes reversal from negative to positive. The underlying reason for the observed difference in the zeta potential between DNA/DTAB and DNA/SD complexes is attributed to the role of SWNTs in binding interactions. At higher weight ratios, DTAB molecules emanate radially from the SWNT sidewalls (see Fig. 2b) and maintain their micelle-like structure while adsorbing onto DNA via electrostatic attractions. This proposed scheme is plausible because of the electrostatic repulsion between the cationic head groups and the hydrophobic interaction between DTAB tails and SWNT. In the course of the complex formation, some head groups of DTAB on SD are attached to one DNA, others to another DNA. With increasing weight ratio and beyond the I.E.P, the electrostatic repulsion overwhelms attraction and the number of unbound SD gradually increases. The positive zeta potential (+53 mV) of the free SD contributes to the increase in the overall zeta potential of the DNA/SD complex at higher SD concentration as shown in Fig. 10b.

Next, we evaluate the hydrodynamic diameter of the DNA/SD complex. At a low weight ratio, DTABs and SWNTs are dissociated from SD because of dilution with DNA. Here, the binding occurs due to the random electrostatic interactions between the free DTA^+ and the phosphate groups of DNA. Since the exterior surface of the ds-DNA is hydrophilic, the SWNTs can interact only with the hydrophobic DNA end base pair planes. The DNA/SD complex exhibits a larger hydrodynamic diameter than the DNA/DTAB complex at the weight ratio below 100 suggesting that the association of isolated SWNTs with DNA end groups contributes to the increase in the complex size. The SD concentration increases up to the I.E.P, and that is where the largest complex size is observed. Jing et al. [69] studied phase behavior of DNA with cationic/nonionic surfactant mixtures and showed no significant hydrophobic association at high DNA concentration indicating no cooperative binding of surfactants due to their predominantly electrostatic interaction with DNA. Their results are in agreement with ours because the effect of SWNTs on the charge neutralization and reversal appears negligible at higher DNA concentration but becomes gradually more significant at lower DNA concentration due to the strong hydrophobic association of SWNTs with DTAB, leading to larger hydrodynamic diameter of the complex. Moreover, a considerably larger size of the DNA/SD complex suggests that the electrostatic attractions between SD and DNA are stronger than the hydrophobic interactions between DTAB molecules, resulting in the SWNT mediated growth of the complex. As the weight ratio increases further, the electrostatic repulsion becomes a dominant force leading to the decrease in the hydrodynamic diameter of both DNA/DTAB and DNA/SD complexes. The above observations support the tenet that the overall complex formation is electrostatically controlled.

3.5. Secondary DNA structure in the complex

We next turn attention to the effect of SWNTs on the three-dimensional helical structure of DNA. The native 'B-form' DNA helix has a unique circular dichroism (CD) spectrum that consists of positive and negative bands near 275 nm and 245 nm, respectively [34,70,71]. The shift of those bands and the change in their spectral shape indicate the rearrangement of the helical structure of DNA. We employed circular dichroism (CD) spectroscopy to determine if any alterations in the secondary structure of DNA were realized in the DNA/SD and DNA/DTAB complexes. The observed signals arise from the DNA molecules because SWNT and DTAB do not possess a significant CD signal within the tested UV region. The measured CD spectra were converted from a unit of millidegree (mdeg) to a universally-comparable unit (mean-residue-molar-ellipticity, deg cm^2/dmol) using the following equation:

$$\theta_M = \frac{100 \cdot \theta \cdot M_w}{c \cdot l \cdot N_r} \quad (4)$$

where θ_M is the mean-residue-molar-ellipticity in deg cm^2/dmol; θ is the experimental ellipticity in mdeg; M_w is the molecular weight of DNA in dalton; c is DNA concentration in mg/mL; l is cuvette path length in cm; N_r is the number of residues of DNA.

As shown in Fig. 11, the spectrum of the neat (uncomplexed) calf-thymus DNA shows a typical B-type conformation with a long-wave positive band at 275 nm and a short-wave negative peak at 245 nm of comparable intensities, with the signal crossing over at the absorption maximum (260 nm). However, the spectra for DNA/SD and DNA/DTAB complexes at various weight ratios exhibit an apparent shift of the two major bands. The decrease in intensity is attributed to the variation in the DNA concentration in both complexes. The change in molar ellipticity demonstrates that the structure of DNA is disturbed by the interactions with DTA^+ and SWNT. In most cases, we observe a shift of negative and positive bands to longer wavelengths with increasing weight ratio (SD:DNA

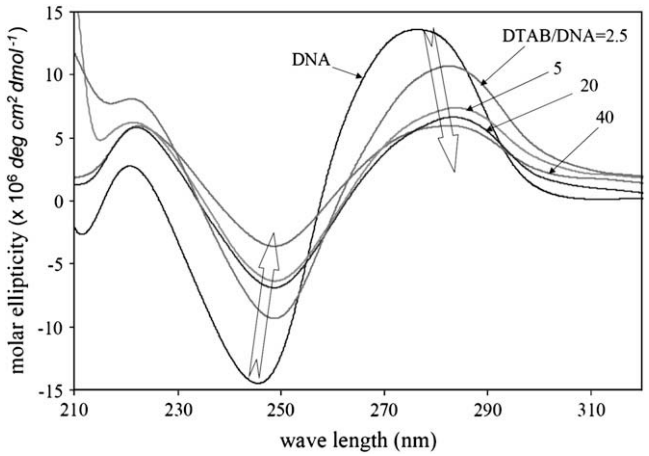

Fig. 11. Molar ellipticity of DNA obtained by CD spectroscopy in DNA/DTAB complexes with weight ratio (DTAB:DNA) as a variable.

or DTAB:DNA). We also note that the CD spectra of DNA in both complexes change with concentration (DTAB or SD) but these changes are not accompanied by the conformational transition from B to A or B to Z form. A careful examination of the FTIR spectra shows that the major marker band for the B-type DNA at 835 cm^{-1} exhibits a small shift of about 5 cm^{-1} to higher wavenumber. This suggests

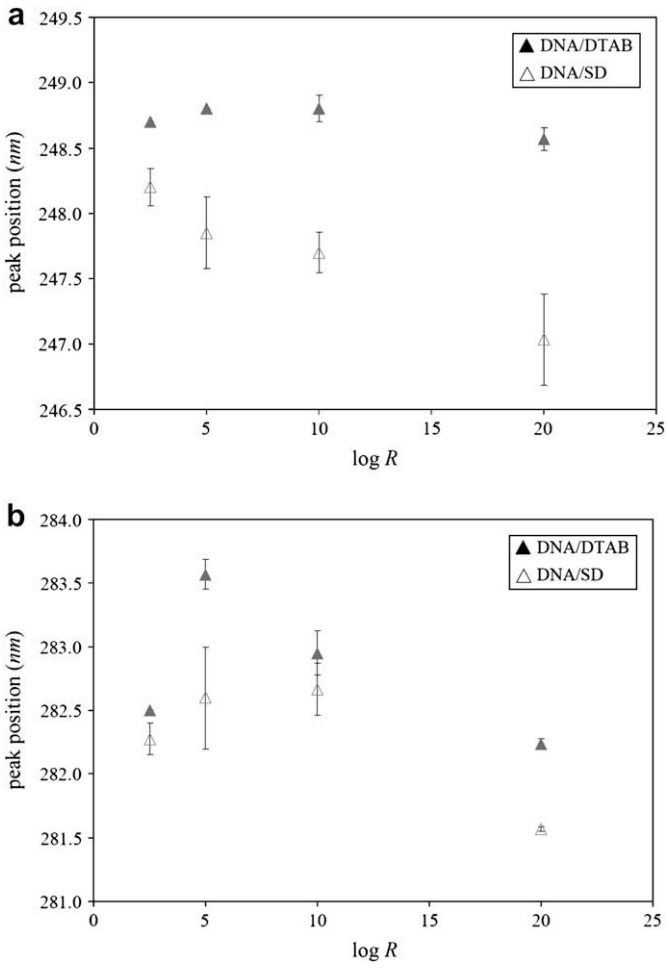

Fig. 12. Variation of (a) negative and (b) positive CD bands in DNA/DTAB (filled symbols) and DNA/SD (open symbols) complexes as a function of weight ratio *R* (DTAB:DNA or SD:DNA).

that the DNA remains in the B-type conformation [36]. Furthermore, the characteristic band of the A-type DNA is known to have a strong negative ellipticity signal at about 210 nm, but we see no evidence of it in our experimental matrix that would suggest transition from B to A or B to Z form [72]. We attribute the changes in the CD spectra to the local perturbations in the DNA base geometry rather than the alterations in the helical structure of DNA [73].

Finally, we examine the effect of hydrophobic interaction between SWNT and DNA on the CD spectra. Fig. 12a and b shows the peak position of positive and negative bands at 275 and 245 cm^{-1}, respectively, as a function of weight ratio for the DNA/SD and DNA/DTAB complexes. The location of both peaks is shifted to longer wavelength in DNA/DTAB than DNA/SD complex, suggesting that the CD spectra are affected more by DTA^+ in the absence of SWNTs. The shift in the peak position demonstrates the role of SWNTs during the complex formation qualitatively but does not contradict the FTIR results because the CD spectra depend on the charge ratio, complex size, degree of DNA compaction and other factors, under circularly polarized light. It is fair to say, however, that the association of SWNT with DTAB makes a difference in the degree of disturbance of the DNA secondary structure.

4. Conclusions

We have completed an investigation of molecular interactions and dynamics in bio-nano complexes of DNA with: 1) cationic surfactant (DTAB), and 2) DTAB wrapped single-walled carbon nanotube (SWNT). These two complexes are denoted as DNA/DTAB and DNA/SD, respectively.

Binding of DTAB to DNA was confirmed by infrared spectroscopy. The extent of binding depends on the DTAB concentration and the spectra reveal a shift to higher wavenumber and a decrease in intensity of all major DNA absorption bands in both complexes. The calculated binding constants for absorptions at 1709 and 1086 cm^{-1} were higher for DNA/SD than DNA/DTAB complex. The higher affinity of SD than DTAB toward DNA is the consequence of electrostatic interaction and topology. The micelle-like topology of SD, where DTAB molecules emanate radially and outward from the nanotube surfaces increases the number of potential binding sites.

The time scale of the dielectric response in both DNA complexes decreases with increasing SD or DTAB concentration, goes through a minimum and then increases. Apparently there exists a specific weight ratio where the process is fastest. This is an interesting finding that we attribute to the variation in non-uniformity of the counterion cloud that surrounds the complex. Fastest relaxation occurs at the highest polarizability and the induced dipole moment. The gradual decrease of binding energy with increasing weight ratio indicates that the binding of DTAB or SD to DNA is favored leading to lower activation energy and a more stable complex.

The role of SWNTs in binding interactions is evident from the measurements of the zeta potential and the hydrodynamic diameter. The major difference in the zeta potential between DNA/DTAB and DNA/SD complexes at higher weight ratio is attributed to the fact that the free DTAB molecules do not contribute to the positive zeta potential but SD do. At a low weight ratio some SWNTs dissociate from the SD complex and interact with the DNA end base pair planes hydrophobically. Larger hydrodynamic diameter of DNA/SD (than DNA/DTAB) complex at lower weight ratio supports the tenet that SWNTs interact with the DNA end groups. In addition, a much larger size of the DNA/SD (than DNA/DTAB) complex at the iso-electric point suggests that the electrostatic attractions between SD and DNAs are stronger than the hydrophobic interactions between the DTAB bi-layers resulting in the SWNT mediated growth of the complex. This implies that the overall complex formation is electrostatically controlled.

The secondary structure of DNA is disturbed by the interaction with DTA^+ as well as SWNT. However, there is no evidence of the conformational transition from type B to other types indicating that these spectral changes are due to the local perturbations in DNA base geometry rather than the alterations in the helical structure of DNA. Interestingly, the CD spectra of DNA are more affected by DTA^+ in the absence of SWNTs suggesting that the association of SWNT with DTAB makes a difference regarding the perturbation of the DNA secondary structure.

Acknowledgement

This material is based on work supported by National Science Foundation under Grant DMR-0346435.

References

[1] Taton T, Mirkin C, Letsinger R. Science 2000;289:1757–60.
[2] Cui Y, Wei Q, Park H, Lieber C. Science 2001;293:1289–92.
[3] Chen R, Bangsaruntip JS, Drouvalakis KA, Kam MWS, Shim M, Li Y, et al. Proc Natl Acad Sci U S A 2003;100:4984–9.
[4] Alivisatos P. Nat Biotechnol 2004;22:47–52.
[5] Kim S, Lim YT, Soltesz EG, Grand AM, Lee J, Nakayama A, et al. Nat Biotechnol 2004;22:93–7.
[6] Gao Z, Wasylishen RE, Kwak JCT. J Phys Chem 1990;94:773–6.
[7] Pattarkine MV, Ganesh KN. Biochem Biophys Res Commun 1999;268:41–6.
[8] Dias RS, Svingen R, Gustavsson B, Lindman B, Miguel MG, Akerman B. Electrophoresis 2005;26:2908–17.
[9] Endres RG, Cox DL, Singh RRP. Rev Mod Phys 2004;76:195–214.
[10] Kotz J, Kosmella S, Beitz T. Prog Polym Sci 2001;26:1199–232.
[11] Gorelov AV, Kudryashov ED, Jacquier JC, McLoughlin DM, Dawson KA. Physica A 1998;249:216–25.
[12] Dias R, Melnikov S, Lindman B, Miguel MG. Langmuir 2000;16:9577–83.
[13] Hayakawa K, Kwak JCT. Cationic surfactants: physical chemistry. New York: Marcel Dekker; 1991.
[14] Kam NWS, Jessop TC, Wender PA, Dai H. J Am Chem Soc 2004;126:6850–1.
[15] Cherukuri P, Bachilo SM, Litovsky SH, Weisman RB. J Am Chem Soc 2004; 126:15638–9.
[16] Bianco A, Kostarelos K, Partidos CD, Prato M. Chem Commun 2005;5:571–7.
[17] Li J, Ng HT, Cassell A, Fan W, Chen H, Ye Q, et al. Nano Lett 2003;3:597–602.
[18] Merkoci A. Mikrochim Acta 2006;152:157–74.
[19] Katz E, Wilmer I. ChemPhysChem 2005;5:1084–104.
[20] Jeng ES, Moll AE, Roy AC, Gastala JB, Strano MS. Nano Lett 2006;6:371–5.
[21] Hwang ES, Cao C, Hong S, Jung HJ, Cha CY, Choi JB, et al. Nanotechnology 2006;17:3442–5.
[22] Becker ML, Fagan JA, Gallant ND, Bauer BJ, Bajpai V, Hobbie EK, et al. Adv Mater 2007;19:939–45.
[23] Zheng M, Jagota A, Semke ED, Diner BA, McClean RS, Lustig SR, et al. Nat Mater 2003;2:338–42.
[24] Zheng M, Jagota A, Strano MS, Santos AP, Barone P, Chou G, et al. Science 2003;302:1545–8.
[25] Feazell R, Rodney P, Nozomi NR, Hongjie D, Stephen JL. J Am Chem Soc 2007; 129:8438–9.
[26] Liu Y, Wu DC, Zhang WD, Jiang X, He CB, Chung TS, et al. Angew Chem Int Ed 2005;44:4782–5.
[27] Cyranoski D, Baker M. Nature 2008;452:132.
[28] Xin H, Woolley AT. Nanotechnology 2005;16:2238–41.
[29] Mijovic J, Lee HK, Kenny J, Mays J. Macromolecules 2006;39:2172–82.
[30] Mijovic J, Han Y, Sun M. Macromolecules 2002;35:6417–25.
[31] Mijovic J, Sy JW. Macromolecules 2000;33:9620–9.
[32] Hsu WL, Chen HL, Liou W, Lin HK, Liu WL. Langmuir 2005;21:9426–31.
[33] Lee SL, Debenedetti PG, Errington JR, Pethica BA, Moore DJ. J Phys Chem B 2004;108:3098–106.
[34] McLoughlin D, Delsanti M, Albouy PA, Langevin D. Mol Phys 2005;103:3125–39.
[35] Sukhorukov GB, Montrel MM, Petrov AI, Shabarchina LI, Sukhorukov BI. Biosens Bioelectron 1996;11:913–22.
[36] Ouameur AA, Tajmir-Riahi HA. J Biol Chem 2004;279:42041–54.
[37] Neault JF, Tajmir-Riahi HA. J Biol Chem 1997;272:8901–4.
[38] N'soukpoe-Kossi CN, St-Louis C, Beauregard M, Subirade M, Carpentier R, Hotchandani S, et al. J Biomol Struct Dyn 2006;24:277–83.
[39] Ouameur AA, Nafish S, Mohajerani N, Tajmir-Riahi HA. J Biomol Struct Dyn 2003;20:561–5.
[40] Li X, Peng Y, Qu X. Nucleic Acids Res 2006;34:3670–6.
[41] Zhao Z, Johnson JK. J Am Chem Soc 2007;129:10438–45.
[42] Shikata TS, Imai I. Langmuir 1998;14:6804–10.
[43] Dintzis HM, Oncley JL, Fuoss RM. Proc Natl Acad Sci U S A 1954;40:62–70.
[44] Sakamoto S, Hayakawa R, Wada Y. Biopolymers 1979;18:2769–82.
[45] Minoura I, Muto E. Biophys J 2006;90:3739–48.
[46] Oosawa F. Polyelectrolytes. New York: Dekker; 1971.
[47] Sun M, Pejanovic S, Mijovic J. Macromolecules 2005;38:9854–64.
[48] Gabriel G, Grant E. Bioelectromagnetics 1999;20:40–5.
[49] Auty RP, Cole RH. J Chem Phys 1952;20:1309–14.
[50] Manning GS. J Chem Phys 1969;51:934–8.
[51] Manning GS. Acc Chem Res 1979;12:443–9.
[52] Kremer F, Schonhals A. Broadband dielectric spectroscopy. Berlin: Springer-Verlag; 2003.
[53] Havriliak S, Negami S. J Polym Sci 1966;C14:99–117.
[54] Havriliak S, Negami S. Polymer 1967;8:161–210.
[55] Havriliak Jr S-, Havriliak S. Dielectric and mechanical relaxation in materials. Munich: Hanser Publ; 1997.
[56] Böttcher CJF, Bordewijk P. Theory of electric polarization. Amsterdam: Elsevier; 1978.
[57] Stevens M. Biophys J 2001;80:130–9.
[58] Mandel M, Odijk T. Annu Rev Phys Chem 1984;35:75–108.
[59] Manning GS. Q Rev Biophys 1978;11:179–246.
[60] Liu H, Gapinski J, Skibinska L, Patkowski A, Pecora R. J Chem Phys 2000; 113:6001–10.
[61] Bohm KJ, Mavromatos NE, Michette A, Stracke R, Unger E. Electromagn Biol Med 2005;24:319–30.
[62] Dewarrat F, Calame M, Schonenberger C. Single Mol 2002;3:189–93.
[63] Bordi F, Cametti C, Colby RH. J Phys Condens Matter 2004;16:R1423–63.
[64] Khachatourian AVM, Wistrom AO. J Phys A Math Gen 2003;36:6495–508.
[65] Matulis D, Rouzina I, Bloomfield VA. J Mol Biol 2000;296:1053–63.
[66] Ni JX. New J Chem 1999;23:1071–3.
[67] Mel'nikov SM, Segeryev VG, Yoshikawa K. J Am Chem Soc 1995;117:2401–8.
[68] Mel'nikov SM, Segeryev VG, Yoshikawa K, Takahoahi H, Hatta I. J Chem Phys 1997;107:6917–24.
[69] Jing D, Zhang J, Ma L, Zhang G. Colloid Polym Sci 2004;282:1089–96.
[70] Lobo BA, Vetro JA, Suich DM, Zuckermann RN, Middaugh CR. J Pharm Sci 2003;92:1905–18.
[71] Gray DM, Ratliff RL, Vaughan MR. Method Enzymol 1992;211:389–405.
[72] Marty R, Ouameur AA, Neault JF, Nafisi S, Tajmir-Riahi HA. DNA Cell Biol 2004;23:135–40.
[73] Braun CS, Jas GS, Choosakoonkriang S, Koe GS, Smith JG, Middaugh CR. Biophys J 2003;84:1114–23.